SCIENTIFIC REPORTS

OPEN

SUBJECT AREAS:
CARBON NANOTUBES AND FULLERENES
CHEMICAL ENGINEERING
POLYMER SYNTHESIS

Received
11 October 2013

Accepted
30 December 2013

Published
4 February 2014

Correspondence and requests for materials should be addressed to K.K.K.K. (kk292@cam.ac.uk)

Ultra-pure single wall carbon nanotube fibres continuously spun without promoter

Catharina Paukner & Krzysztof K. K. Koziol

Department of Materials Science and Metallurgy, University of Cambridge, 27 Charles Babbage Road, CB3 0FS Cambridge UK.

We report a new strategy towards the control of carbon nanotube (CNT) structure and continuous fibre formation using a floating catalyst direct spinning CVD process. In the procedures used to date, a sulphur promoter precursor is added to significantly enhance the rate of CNT formation in the floating catalyst synthesis. Within the reaction zone, the rapidly grown nanotubes self-assemble into bundles, followed by their continuous spinning into fibres, yarns, films or tapes. In this paper we demonstrate a catalyst control strategy in the floating catalyst system, where the CNT formation process is independent of the presence of a promoter but leads to successful spinning of the macroscopic carbon nanotube assemblies with specific morphology, high purity (Raman D/G 0.03) and very narrow diameter range (0.8–2.5 nm). This can be achieved by the control of catalyst precursor decomposition and subsequent formation of homogeneous nano-sized catalyst particles.

Carbon nanotubes are essentially hollow tubes, of a honeycomb wall structure from solely carbon atoms[1]. There is particular interest in single wall carbon nanotubes (SWNTs) as they show remarkable electrical and electronic properties, combining either metallic or semi-conducting behaviour (with tunable band gap), very low density and high mechanical performance[2]. In order to create a macroscopic material preserving the unique properties of the individual carbon nanotubes, it would be necessary to avoid any intermediate processing steps, which often introduce topological defects and substantially shorten the length of individual nanotubes. The direct spinning process relies on various important parameters which ensures uninterrupted synthesis[3,4]. In this process, the reaction time for the generation of active species and their role in the formation of nanotubes takes approximately 3 seconds. In the cases of process scale up one requires to use higher furnace temperatures to guarantee a sufficient energy transfer to the precursor substances compared to the time available in substrate growth setups[4,20]. Furthermore the complexity of the process and rapid synthesis can lead to instabilities and formation of undesirable carbonaceous and metallic impurities, interfering with the realisation of macroscopic materials with the outstanding properties of individual CNTs[4].

Since the early times of direct CVD CNT fibre spinning from various carbon sources (including ethanol, hexane and methane) as well as ferrocene (iron catalyst source), a sulphur compound was always required to activate the iron catalyst particles[3]. Sulphur is known to form stable bonds with iron, thereby demobilizing the catalyst on the surface and preserving the particle in its current size and guaranteeing a narrow size distribution of the iron nanoparticles. Iron atoms become available from their ferrocene precursor from about 400°C[4,5] and start to collide in the reactor tube. During the time until carbon becomes available for reaction, the growth of iron particles by coalescence of the atoms is uncontrolled and produces a variety of sizes in iron clusters. Due to its high stability, CH_4 (methane) has a comparatively high pyrolisation temperature and thus carbon only becomes available for reaction with the transition metal at around 1200°C[6]. In order to keep these clusters small and in a narrow size range, sulphur compounds such as thiophene, carbon disulphide and others have been applied[7–9]. These less stable hetero compounds were chosen to release sulphur at temperatures similar to ferrocene pyrolisation[4]. Due to their high vapour pressure these sulphur compounds however are difficult to dose. Too much sulphur present for the reaction entirely encapsulates iron and thus hinders its catalytic activity completely, which leads to soot formation and impurities, which in turn create holes and weak spots in the fibre. As a result, an excessive amount of very short, unaligned tubes are formed around the catalyst particles, commonly referred to as "impurities". The presence of short and purely formed nanotubes cause generally higher defect induced peaks in the Raman spectra. Moreover, S compounds suitable for the spinning process generally show a high toxicity for

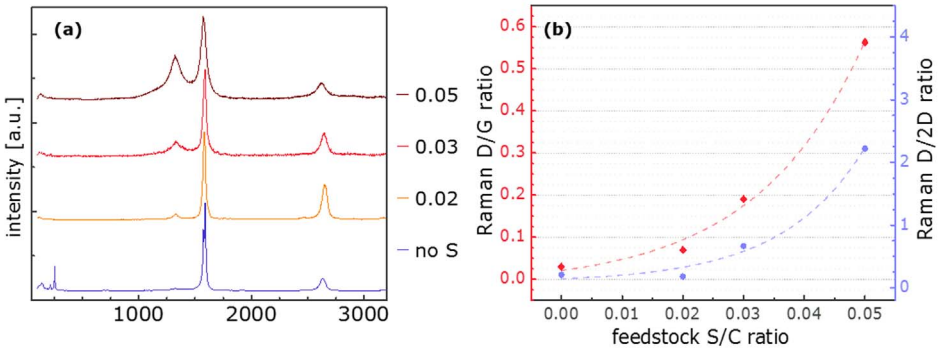

Figure 1 | (a) Raman spectra of CNT fibre generated from toluene and ferrocene with (S/C ratio shown in the legend) and without thiophene normalised to the G peak (G = 1), offset along the y axis and (b) correlation between S/C ratio in the reaction feedstock and the D/G intensity ratio (red, linear) and the D/2D intensity ratio (blue, exponential) in Raman spectroscopy on the resulting fibre.

humans, particularly the hazard of reproductive damage, including impairing fertility[10,11]. Therefore, developing a process without any S utilization is highly desirable.

Results of the present study show that CNT fibre spinning can be performed successfully without sulphur precursors avoiding the aforementioned drawbacks. To the knowledge of the authors, this paper is the first to report that SWCNT fibre spinning is also possible without sulphur as a promoter, in fact without addition of any sort of heteroatom additive, like sulphur, nitrogen or oxygen. The aim of the study is to show the effects of avoiding sulphur on the morphology of the CNT fibres using a precursor system of toluene and ferrocene. Beside the fact that this process provides a less toxic way to form CNT fibres from fewer ingredients than those reported so far[4,12], the resulting material shows to be cleaner and at optimised conditions made from long bundles of SWCNTs.

Results

Sulphur effect. In an initial set of experiments a fibre consisting of CNTs could be spun for the first time without addition of heteroatom additive. In this series of experiments the amount of additive was gradually decreased culminating in fibre spinning from a feedstock of ferrocene and toluene only. The injection temperature was constant at 330 ± 5°C. Moreover, Raman spectra of samples normalised to the G peak impressively show how the addition of thiophene creates defects or impurities in the CNT based fibre (Figure 1a). Figure S1 shows the same Raman spectra normalised to the D peak, highlighting the change in the G peak in terms of both intensity and shape as the sulphur amount in the feedstock is decreased. While samples from 2 or 3% sulphur in the feedstock show Gaussian peaks with good separation of G and D peak, increase to 5% S shows less defined separation and a clear increase in D and decrease in 2D peak intensities. The removal of sulphur however brings a remarkable change as the G intensity (1589 cm^{-1}) increases by about 4 times and clearly splits off a separate peak at 1573 cm^{-1} (Figure S1b). Moreover, RBM peaks are visible with a main intensity at 254.0 cm^{-1}.

As can be seen in Figure 1b), an exponential correlation was found between the sulphur amount present for the reaction and the D/G ratio, indicating defects, ie sp^3 hybridized carbon atoms, in the respective Raman spectra (summarised in Table S1). While fibre from an injection feedstock containing 5% sulphur shows a massive D peak, creating a D/G ratio of 0.56, it decreases with decreasing thiophene amounts and shows an almost negligible (0.05) D/G when thiophene injection is stopped. The D/2D ratio displays an exponential dependence on the sulphur content in the feedstock with values around 0.2 for up to 2% and 0.7 for 3% sulphur. Increase to 5% sulphur yields in reversed intensities of these two peaks leading to a D/2D ratio of 2 (Figure 1b, Table S1).

This data is consistent with the SEM images (Figure 2a and b) where it is clearly seen that a significant amount of blob like impurities are incorporated into an aligned network of CNT bundles when thiophene was present in the feedstock (Figure 2a). However those from a sulphur-free feedstock show remarkably clean CNT fibre, with well aligned bundles and a negligible amount of impurities visible at the chosen magnification (Figure 2b).

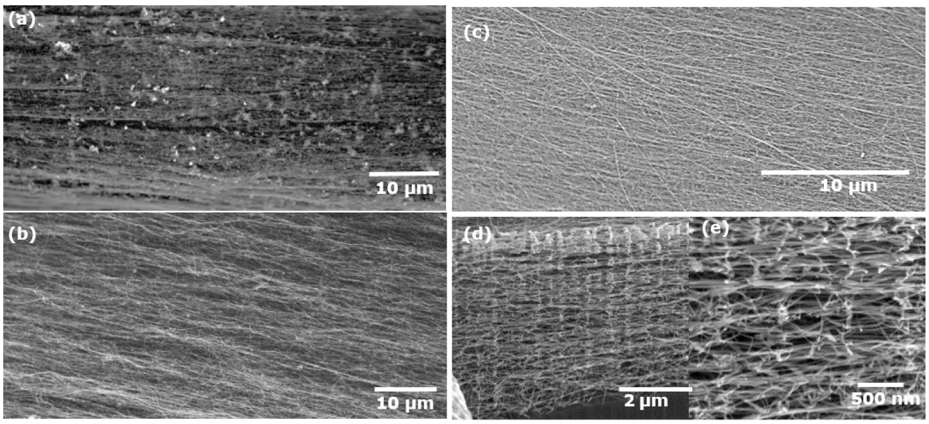

Figure 2 | **SEM images of fibre obtained from toluene, ferrocene (a) with and (b) without thiophene through a single port injector at 15 cm injection depth, (c) at 10 cm injection and corresponding FIB images of sample from 10 cm injection depth cut inside along the fibre axis in (d) and (e) at magnification as indicated.**

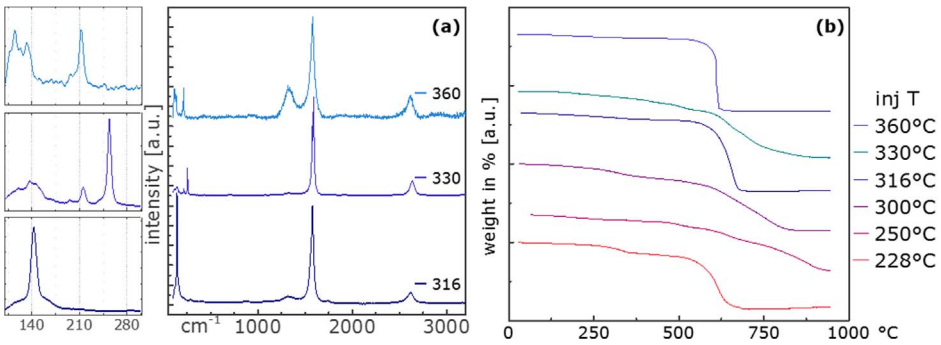

Figure 3 | (a) Raman spectra of CNT fibre samples from 15 cm injection depth normalised to the G peak (G = 1) listed according to their injection temperature (in °C) with zoom in on RBM region and (b) TGA of CNT fibre samples listed according to their injection temperature.

Injection temperature. Following this observation, the effect of the injection temperature on the process from a feedstock of toluene and ferrocene without heteroatomic additives was investigated. In order to explore different injection temperatures the injection depth was decreased from 15 to 10 and 5 cm. This corresponds to injection temperatures between 200 and 360°C as a function of injection depth and carrier gas flow (see Table S2) for our furnace in which the temperature of the reaction zone goes up to 1200°C (temperature profile see Figure S2).

Experiments at 15 cm injection depth showed that fibres were readily produced entirely without heteroatom additive from injection temperatures of 316 ± 5, 330 ± 5 and 360 ± 5°C, respectively (Table S2). Raman spectra of these samples in Figure 3a (normalised to the G peak) show that D/G ratios remain very low, 0.03 and 0.09 up to 330°C. The lowest injection temperature shows the most pronounced RBM peak at 142.9 cm^{-1}, 330°C at 254.0 cm^{-1}. The higher injection temperature shows a significantly different Raman spectrum with D/G of 0.47. RBMs of similar peak intensities are observed at 114.5, 132.3 and 211.9 cm^{-1}.

Normalisation to the D peak (D = 1) in Figure S3 displays more clearly the difference in the G peaks in both shape and intensity. Both samples from 316 and 360°C show a single Gaussian G peak, the sample from 330°C is split in the aforementioned 1589 cm^{-1} and 1573 cm^{-1}. The 2D peak intensity is highest for the sample from 330°C (D/2D 0.21) and poor for 360°C (D/2D 1.33) (data summarised in Table S3).

In decreasing the injection depth, we found that CNT fibre could also be spun successfully from injection at 10 cm. Injection at 5 cm did not yield spinning of CNT fibre. The material displays almost no surface impurities. Interestingly, the Fe/C ratio that lead to successful spinning was very similar for all samples even though the absolute amounts of precursors injected for reaction were varied between 0.5–2.2 mmol C/min. More or less independent of the injection temperature, the ideal Fe/C ratio was found to be 0.031 ± 0.003 in all cases, so an order of magnitude higher than with injection at 15 cm. As shown before for experiments at an injection depth of 15 cm and corresponding higher injection temperatures between 315 and 360°C, significantly lower (below 0.002) Fe/C ratios lead to successful fibre formation.

Thermo gravimetric analysis (TGA) was performed subsequently in order to gain information about the composition of the bulk material. Analysis of iron contents of the various samples shows generally significantly lower residues for samples from higher injection temperatures. Whereas iron contents in samples from injection at 15 cm with Fe/C ratios below 0.002 in the feedstock was found to be between 0.3–7.4 wt%, substantially higher values of 15 and 30 wt% were found for those from 10 cm and Fe/C ratios around 0.03. In the TGA spectra shown in Figure 3b, different weight loss behaviours could be observed. From TGAs of samples no clear correlation between injection temperature and purity and morphology of the CNTs could be detected. A direct correlation of impurities other than iron and iron remaining in the sample could not be identified.

The corresponding Raman spectra in Figure 4a reveal the following trends for injection at 10 cm: RBMs are present along the entire range of injection temperatures but vary in intensity and Raman shift (summarised in Table S3). While the spectrum of the sample from 300°C injection temperature shows its most pronounced RBM peak at around 150.0 cm^{-1} (Figure 4a inset, Table S3) lowering the injection temperature yields peaks around 210 ± 15 cm^{-1}. According to the aforementioned wavenumber-tube diameter correlation ($d = 223/(\omega - 10)$)[13] these wavenumbers correspond to tube diameters of 1.67 nm and 1.26–1.09 nm.

To a good approximation both D/G and D/2D ratio are exponentially decreasing with increasing injection temperature as can be seen in Figure 4b.

In order to get a better impression of CNT features within different samples, electron microscopic investigations were performed (for clarity, sample characteristics and synthesis parameters are

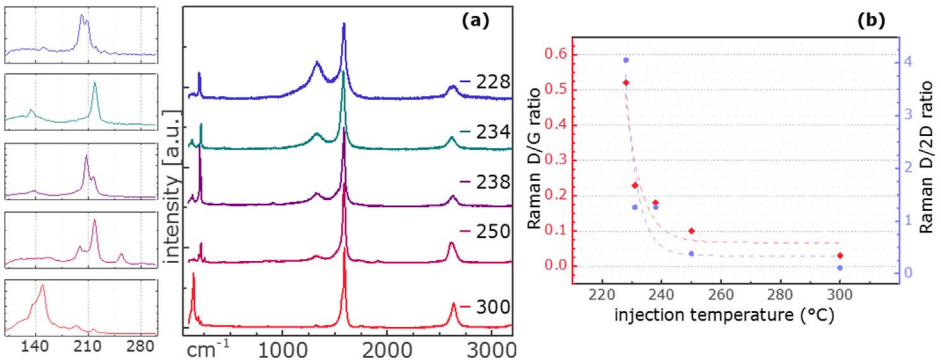

Figure 4 | (a) Raman spectra normalised to G for 10 cm injection depth listed according to their injection temperature with a zoom-in on each RBM region; (b) exponential correlation between injection temperature and D/G ratio (red squares) and D/2D ratio (blue dots) in the same samples.

Table 1 | Properties of sample selection for HRTEM imaging

	inj. T (°C)	D/G	Fe (%)	diam (nm)
15_1	360	0.09	2.6	3–18
10_2	228	0.41	15	4–17
10_3	300	0.03	15	0.8–2.5

summarised in Table S3). We aimed at characterising the entire bandwidth of injection temperatures and are exemplarily presenting the both extremes and the centre point. Findings of a sample obtained at an injection depth of 15 cm (inj. T 360°C), (hereafter referred to as 15_1) were compared to samples from 10 cm injection depth (hereafter referred to as 10_2 and 10_3 respectively) and a corresponding injection temperature of 228°C and 300°C (Table 1). TGA and Raman spectra determined our expectations for investigation with HRTEM. This way, 15_1 with comparatively low Fe content (2.6 wt%) and no low-burning impurities could be compared with 10_2 where in addition to an above average Fe content of 15 wt%, polymeric impurities were present, indicated by a TGA peak at around 340°C and the high D/G ratio of 0.52. As described earlier, Raman spectra of samples from 10 cm injection depth primarily show RBM peaks, around 150 (10_3) or 210 cm^{-1} (10_2) respectively whereas 15_1 shows two peaks (114.5 and 211.9 cm^{-1}). Interest in investigating the former more closely, additionally came from its very low D/G ratio (0.03).

Sample 15_1 shows a single sharp weight loss peak in TGA (Figure 3b) and impurity free surfaces (Figure 5a). More surface impurities are visible for 10_2 (Figure 5b), which also shows a broader weight loss region in TGA. Sample 10_3 finally shows the highest amount of impurities on the surface (Figure 5c, Figure S5 for a low magnification image of the fibre), which is reflected in a very broad weight loss region in TGA (Figure 3b). To demonstrate that these impurities are concentrated mainly on the surface however, Figure 2d, e shows the highly pure interior of the product, exemplified by FIB images taken from sample 10_2. In Figure 5d, a TEM-BF image taken of sample 15_1 shows fibre strands with small iron particles incorporated in good agreement with the iron residue found in TGA (3%). The sample reveals single wall adjuncts of varying diameter (Figure 5e) on the predominant larger diameter tube network as well as collapsed tubes (Figure 5f). These adjuncts were not considered upon determination of tube diameter distribution (3–18 nm, Figure 5g).

Figure 6 shows the HRTEM images from sample 10_2 revealing mostly multi wall tubes with amorphous material incorporated in the graphene layer system. CNT diameters vary between 4 and 17 nm.

Finally, sample 10_3 shows a big step forward in CNT diameter control. As shown in Figure 7, nicely aligned bundles of SWNTs could be observed in this sample obtained from a higher injection temperature of 300°C. Figure 7d reveals that these SWNTs possess a mean diameter of 1.50 nm and a fairly narrow distribution between 0.7 and 2.75 nm.

Discussion

Sulphur effect. From findings in the first set of experiments with altered sulphur content in the feedstock (Figure 1), its excessive levels in the synthesis zone have a negative effect on the resulting material. The increase in D peak intensity Raman spectroscopy shows clear evidence for an increase in impurities and defects with thiophene in the feedstock. Similarly the lowering of the 2D peak indicates distortions resulting in a lack of resonance within the CNT graphitic lattice. A possible explanation for this is that sulphur forms a coating on the iron particles[14]. This hinders carbon diffusion into the inner parts of the metal which makes it faster available for incorporation into the forming honeycomb structure which is supported by the observation of slightly lower spinning rates as thiophene is removed from the injection system going down from 60 m/min to 40 m/min. In the case of over-injection however this coating poisons the iron particles, making them unavailable for catalysis. They stay in the sample as impurities, creating defective islands of metal in the CNT bundle network which in turn also induces a decrease in alignment of the bundles within the fibre. Therefore cleaner fibre results as no sulphur is present in the feedstock. In agreement with previous reports a thiophene/toluene ratio in the feedstock of around 0.25 produces collapsed double wall tubes, providing an explanation for the good D-G peak separation as well as the missing RBMs in the Raman spectra[14]. The impressive increase in G peak intensity combined with a clear separation of G^- for the sample spun without additive, indicates a distinctly different material from the other samples[15].

Injection temperature. It is crucial to note that the heteroatomic additive is not the only potential source of impurities. Floating catalyst CVD is in general a very sensitive method for growing CNTs and will only yield in continuous fibre spinning under very specific ratios of carbon, catalyst and carrier gas (Tables S2, S3).

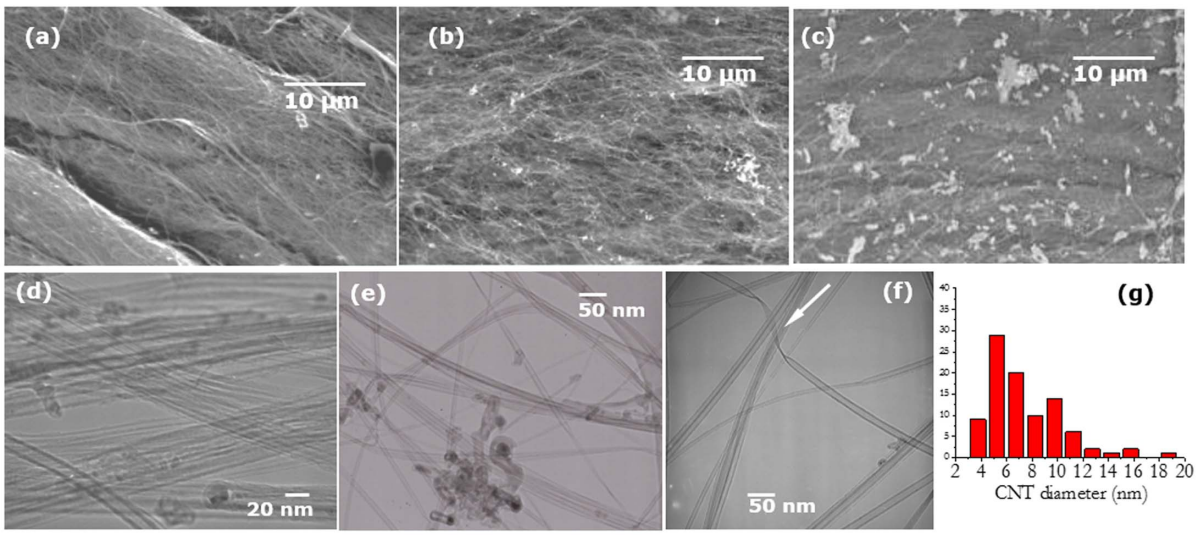

Figure 5 | SEM on samples (a) 15_1, (b) 10_2 and (c) 10_3 and (d) sample 15_1 TEM BF image with catalyst particles incorporated (e) in the network of MW and SWNTs and collapsed tubes (f) (arrow); Corresponding tube diameter distribution in g).

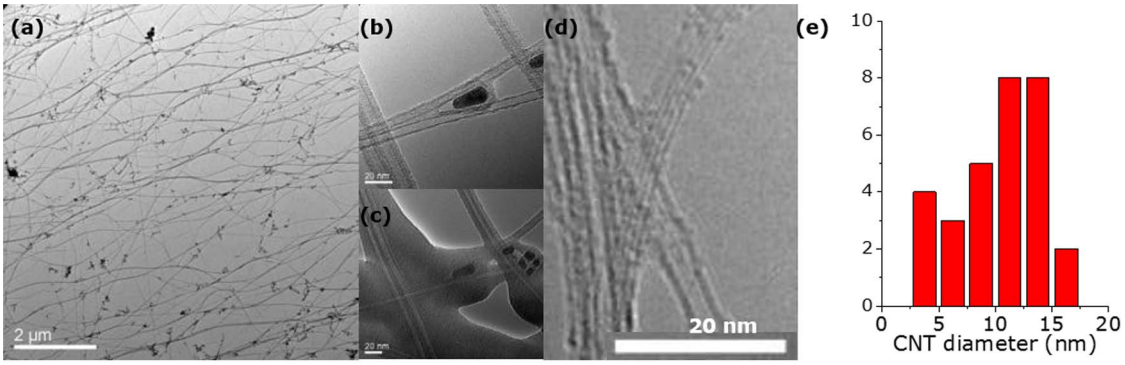

Figure 6 | HRTEM of sample 10_2; (a) overview with network of long MWNT bundles with incorporated impurities, (b) catalyst particle between two growing tubes, amorphous material between defective graphene layers, (c) amorphous material molten under electron beam, d) a bundle of SWNTs and e) the CNT diameter distribution in nm.

Pyrolysis of toluene at lower temperatures matches catalyst availability from ferrocene break-down well and enables CNT formation at an early stage within the reactor. The resulting longer reaction time enables SWCNTs to grow to a length which enables them to bundle up due to van der Waals forces and be extracted as a continuous fibre. Once these feedstock combinations are identified, the morphology of collected samples therefore depends on subtle parameters within the setup. We have been able to identify the injection temperature as one of the most crucial parameters. Apart from the injection depth, this temperature strongly depends on the amount of hydrogen, as well as amount and temperature of the carrier gas stream (helium). The most likely explanation for its significance is its effect on the catalyst precursor. Temperatures higher or close to its pyrolysis point (400°C[4]) within the injector tube start its decomposition already within that confined space of about 4 mm diameter. The shorter mean free path of the evolving iron nanoclusters[4] causes a higher collision and thus coalescence probability. Resulting bigger catalyst particles are believed to generate CNTs with bigger diameters (Figure S7)[16,17]. Agglomerations of these clusters (Figure S4) are not catalytically active for CNT growth and build impurities leading to the observed lower G peak intensity and higher D peak (Figure 3a). Similarly they lower the resonance of CNT bundles resulting in lower 2D peak intensities.

Injection at temperatures well below the pyrolysis of ferrocene should in turn result in smaller catalyst particles and CNTs. However we expect that upon lowering the injection temperature further too high dilution of iron within the reactor gives way to catalyst poisoning by excess carbon and again impurities in the fibre. That injection at 5 cm did not yield any CNT fibre may be a result from a too low injection temperature (below 200°C). It could also be attributed to a convection phenomenon described for the vertical reactor setup[4] probably preventing most of the precursor from advecting into the reaction zone.

The injection temperature affects the morphology of the material obtained from 10 and 15 cm injection depth (Figure 4a). Screening samples across the range from 360 (close to ferrocene pyrolysis) to 220°C, we were able to identify the "turning point", the injection temperature region optimal for small diameter CNT growth with low defects as 310 ± 15°C.

Further valuable information provided SEM and HRTEM investigations (sample properties summarised in Table 1). As observations from sample 15_1 Figure 5d, e reveal, tube diameters vary widely from 3 to approximately 18 nm. The random size distribution suggests little control over the catalyst particle size which can be explained by the high temperature at the point of injection (360°C). Considering that this temperature is close to the pyrolisation temperature of ferrocene (400°C in hydrogen, Figure 8a)[4], it is likely that iron becomes available from the precursor partly already within the injector tube. The shorter mean free path will cause more frequent collision between and thus coalescence of iron atoms to subsequently big but randomly size distributed clusters. Another part of ferrocene will still break up only within the reactor tube, providing an explanation for smaller tubes found in the sample.

It is known that CNTs burn in air between 500–800°C depending on their diameter, number of walls and amount of defects whereby small tubes burn at lower temperatures[18,19]. Apart from different CNT types, polymeric type substances like carbohydrates could be identified by their lower combustion temperatures between 300–425°C. A single sharp weight loss thus indicates the presence of CNTs only with similar diameters without any further carbonaceous impurities which is the case in our samples with iron contents below 3% (15_1). To explain this correlation in more detail, it is crucial to understand that the iron remainder in a sample almost never derives from the catalytically active iron particles. High iron residues therefore stem from poisoned – ie carbon coated - clusters of small metal particles (TEM images in Figure S4). This carbon coating can be of

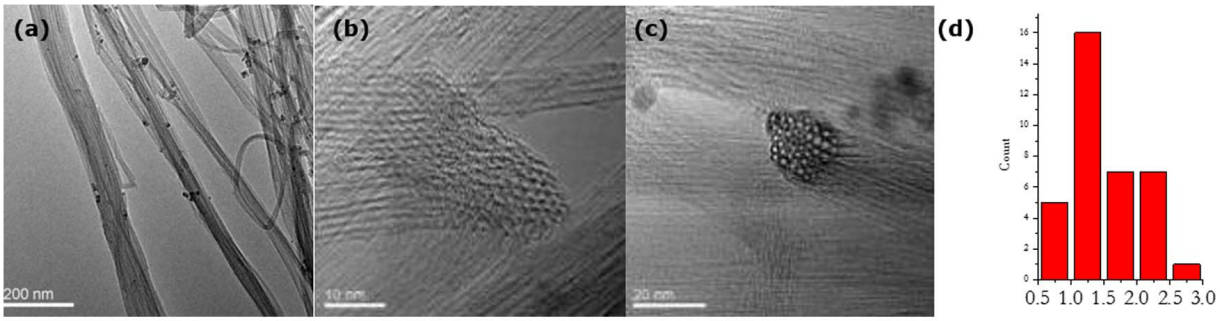

Figure 7 | HRTEM of sample 10_3; a) overview with aligned CNT bundles with incorporated catalyst particles, b) SWNT bundle bend, c) end of a SWNT bundle in top view and (d) CNT diameter distribution in nm.

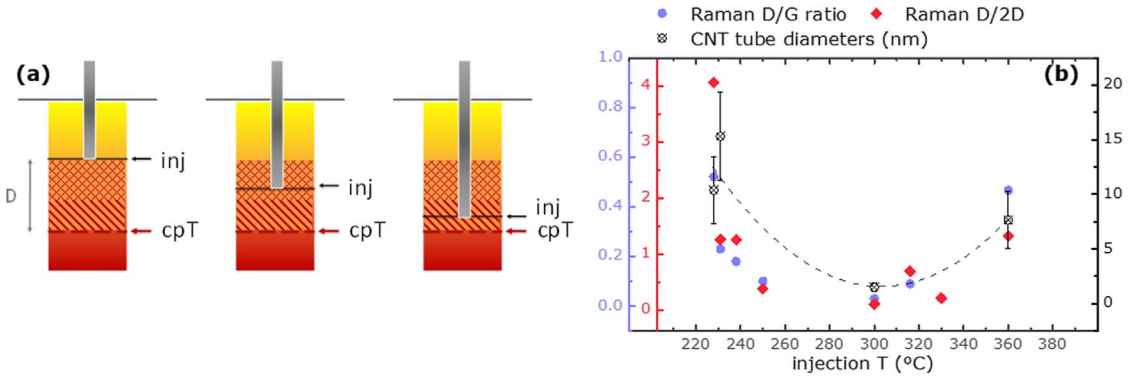

Figure 8 | (a) Catalyst pyrolisation temperature (cpT - at 400°C) with respect to the injection temperature with distance D and (b) correlation of D/G (blue circles) and D/2D (red squares) ratios from Raman spectroscopy and the obtained CNT diameter (black hollow circles) with injection temperature.

graphitic nature, but always requires defects in the hexagon structure to mimic the shape of the almost spherical or oval metal particles. It will therefore be less stable than carbon nanotubes and show as lower temperature impurities. For sample 10_2 Figure 6 b, c impressively show how these melt under the electron beam, which can be correlated with the mass loss observed in TGA around 340°C.

The injection temperature in the case of sample 10_2 was 228°C which is far below the ferrocene pyrolisation temperature. We should expect a long mean free path for iron atoms within the carrier gas stream. Iron clusters will be comparatively small, but potentially also too small to catalyse the reaction to CNTs. These particles will get poisoned by the carbon as it becomes available and should be visible as impurities in the sample (Figure 6a). Randomly distributed bigger clusters of metal should enable the formation of a range of CNTs with potentially wide diameters. Moreover, confirming our assumption in terms of injection temperature, many catalyst particles with various shapes like obelisk, round as well as oval and around them many short tubes can be seen in Figure S4. Together with partly collapsed tubes these provide an explanation for the fairly high D peak in the collected Raman spectra (D/G 0.52). Occasional single wall tubes, shown in Figure 6d, result in observed RBM peaks (Figure 4a). Tube sizes vary evenly between 2 and 16 nm (Figure 6e), offering an explanation for the different pyrolisation behaviour found in the TGA spectrum (Figure 3b).

Combination of comprehensive characterisation of samples shows a good agreement between nanostructure investigations in Raman and TEM, as well as microstructure characterisation in SEM and TGA for sample 10_3, representative for the injection temperature region around 300°C. SEM images (Figure 5c) revealed a number of surface impurities which are believed to be responsible for the various different low-burning substances identified in TGA. It is proposed that this represents the ideal temperature in terms of ferrocene pyrolisation occurring just after injection but not yet within the injector. Iron particles with a narrow particle size distribution could grow to just the right size for being catalytically active but not further yet by the time carbon becomes available from toluene pyrolisation. Supporting this consideration, TEM images in Figure S4 show a number of catalyst particles having almost the same diameter. Moreover, the extremely low disorder found in Raman spectroscopy (D/G 0.03) is supported by TEM images that show barely any impurities apart from superfluous metal particles (Figure 7a) potentially disturbing the structures in the CNT network (Figure 7b, c). The CNT diameter distribution in this sample is narrow between 0.8 and 2.5 nm. Most counts lie between 1 and 1.5 nm in good agreement measured RBM peaks at 150.0 (1.67), 194.1 (1.27) and 217.1 cm^{-1} (1.13 nm) (Figure 4a).

Figure 8a shows pyrolisation of ferrocene (cpT) in relation to the temperature at injection point. At cpT transition metal 400°C iron atoms become available and will start to collide and coalesce into catalytically active clusters. As the distance D between injection and the point of catalyst precursor pyrolisation gets smaller the collision probability between nascent catalyst atoms is higher and the preceding dispersion period of precursor molecules shorter. A higher number of collisions leads to bigger metal clusters. CNTs display diameters that match these metal cluster sizes (Figure S7). As demonstrated above we found that the injection ideally occurs at about 310 ± 15°C which leads to mainly SWNTs building up the fibre (Figure 3a, sample 316°C and sample 10_3 Figure 7). At significantly lower injection temperatures (<230°C) the longer reaction zone yields a wider variety of tube diameters with on average significantly bigger multi wall tubes (Figure 8b, CNT diameter). The greater reactant diffusion also supports formation of by products as demonstrated in Figure 8b, Raman D/G vs. injection temperature. Similarly, bigger diameter CNTs are formed as the injection temperature exceeds its optimal range. The proximity of injection to catalyst pyrolisation temperature leads to a partial break up of catalyst already within the injector pipe. The significantly shorter mean free path within the confinement of the injector stem leads to bigger catalyst clusters. The wide CNT diameter range is explainable by some ferrocene pyrolising within the injector while some of the material does not break up until the bigger volume of the reaction tube.

In this study we show that it was possible for the first time to spin SWCNT fibre (Figure S5) using a continuous floating catalyst CVD process from ferrocene and a carbon source only, without addition of sulphur or any other heteroatomic precursor. The appropriate carbon source for this experimental setup was found to be toluene. The absence of sulphur in the process enhances the purity of the sample. Indicated by very low D/G ratios in Raman spectra of just 0.03, it was possible to spin CNT fibre with almost no impurities such as polymeric structures or encapsulated iron particles. The catalyst structure is correlated with the CNT type formed and could be controlled solely by selecting the appropriate carbon source and adjusting the temperature at the injection point.

Methods

Growth of CNTs and spinning process. In the CNT fibre spinning process described elsewhere[3,4], the vaporized carbon and catalyst precursors are injected at the top of a vertical tube furnace of 1 m heated length and 10 cm diameter using helium as carrier gas. Hydrogen is used at all times in this process. It acts as the reaction medium for the floating catalyst and subsequent formation of the carbon nanotube aerogel in the central hot zone of the furnace which is maintained at 1200°C. In order to allow for continuous extraction of CNT fibres, the furnace is open to the environment at the bottom end. At this point hydrogen is extracted and diluted with inert gas to ensure safety and smooth operation of the spinning process.

The formation of carbon nanotubes in the floating catalyst process is very fast. A typical spinning rate of the CNT fibre is 20 m/min leaving the nanotubes in the furnace for at most 3 seconds. The length of nanotubes averages to about 1 mm[21], which put together with the spinning rate, indicates that the growth of nanotubes

happens in a very short time window. Subtracting the cold zones of the furnace, individual CNTs grow at a rate of about 0.5 mm/sec.

To enable fibre spinning, CNTs have to be long enough to adhere in aligned bundles. This is only then possible if catalyst and carbon precursors break up at a rate fast enough to make the actual reacting species available for nanotube initiation and subsequent growth. An important parameter in the control of the nanotube type is the diameter of the catalyst nanoparticle, which defines the diameter of the resulting nanotube[16,17,22].

Various carbon sources such as methane, ethanol, ethylene and toluene were tested to identify the precursor that would offer the possibility to spin fibre without sulphur addition. These carbohydrates vary in terms of their pyrolisation temperature as well as carbon number per molecule and hybridization. The optimal combination of these parameters to enable spinning without sulphur addition could be identified when toluene was used as the C source. Carbon (toluene), iron (ferrocene) and sulphur precursor (thiophene) together with the hydrogen carrier gas stream were injected via the same pipe (stainless steel pipe of ¼″ OD) at a constant injection depth of 15 cm (ie how far the injector stem reaches into the reactor). Keeping constant both carbon flow at 0.20 mmol/min and Fe/C ratio at 0.002, the sulphur amount was varied from S/C 0.05 to 0.03, 0.02 (atomic ratio) and no sulphur addition. As a result, the effect of thiophene presence in the injection feedstock for CNT fibre synthesis was investigated. In a subsequent set of experiments, the influence of different Fe/C ratios was explored. Here the helium carrier gas flow was varied while the ferrocene temperature was kept constant. Lastly the general effect of varied injection temperature on the fibre morphology of material from a no S feedstock was investigated. For this purpose the injection depth was varied to 10 and 5 cm.

Characterisation. After production, the purity of CNT fibres was investigated using a Renishaw Raman RM2000 spectroscope with 633 nm wavelength of HeNe laser.

Raman spectroscopy is commonly used to demonstrate the structural purity of CNTs based on a peak (G peak) between 1550 and 1600 cm^{-1} which is related to the tangential mode vibrations of the C atoms in hexagonal arrangement. The D peak at 1330 ± 20 cm^{-1} is generated by sp^3 hybridized carbon in the sample[23]. It thus indicates defects present within the lattice as well as extraneous carbonaceous materials. D is related to G leaving a ratio comparable for different batches (D/G ratio). The peak around 2600 cm^{-1} is the double frequency of the D peak, referred to as G′ (for its intensity) or 2D (from its origin). High 2D peaks indicate good resonance within the graphitic lattice, low intensities indicate distortions in the system, eg. doping. It depends on the type of tubes (SW/MW), the number of layers and the quality of graphitisation[24].

Peaks in the region between 100 and 300 cm^{-1} stem from vibrations called radial breathing mode (RBM) as all carbon atoms move in phase orthogonal to the tube axis creating a breathing-like vibration of the entire tube. RBM peaks indicate the presence of single wall CNTs[25]; the diameter of the tubes can be calculated from their wavenumber via $\omega = 223/d + 10$[26,27].

Scanning electron microscopy (SEM; JEOL6340 FEG SEM) and transmission electron microscopy (TEM; FEI Tecnai F20 FEG TEM) were used to analyse the presence of extraneous species and microstructure of CNT samples. Diameters of 60–100 tubes where taken from the images using ImageJ. Thermo gravimetric analysis (TGA, TA Instruments Thermogravimetric Analyser TGA Q500) detects the weight loss of a sample as the temperature increases with a set ramp over a given period of time. It was used to examine the thermal stability, get an idea about the amount of low burning, polymeric material as well as catalyst residues within the fibre. In these tests about 2 mg of sample were placed on a platinum pan and heated up from room temperature to 900°C at a rate of 10°C min^{-1} in 20 mL min^{-1} of air.

1. Iijima, S. Helical microtubules of graphitic carbon. *Nature* **354**, 56–58 (1991).
2. Harris, P. J. F. *Carbon Nanotube Science Synthesis, Properties and Applications.* (Cambridge University Press, 2009).
3. Li, Y.-L., Kinloch, I. A. & Windle, A. H. Direct spinning of carbon nanotube fibers from chemical vapor deposition synthesis. *Science* **304**, 276–278 (2004).
4. Conroy, D., Moisala, A., Cardoso, S., Windle, A. & Davidson, J. Carbon nanotube reactor: Ferrocene decomposition, iron particle growth, nanotube aggregation and scale-up. *Chem. Eng. Sci.* **65**, 2965–2977 (2010).
5. Kuwana, K. & Saito, K. Modeling CVD synthesis of carbon nanotubes: Nanoparticle formation from ferrocene. *Carbon N. Y.* **43**, 2088–2095 (2005).
6. Pinilla, J. L. *et al.* High temperature iron-based catalysts for hydrogen and nanostructured carbon production by methane decomposition. *Int. J. Hydrogen Energy* **36**, 7832–7843 (2011).
7. Stano, K. L. *et al.* Direct spinning of carbon nanotube fibres from liquid feedstock. *Int. J. Mater. Form.* **1**, 59–62 (2008).
8. Koziol, K. K. K., Ducati, C. & Windle, A. H. Carbon Nanotubes with Catalyst Controlled Chiral Angle. *Chem. Mater.* **22**, 4904–4911 (2010).
9. Sundaram, R. M., Koziol, K. K. K. & Windle, A. H. Continuous Direct Spinning of Fibers of Single-Walled Carbon Nanotubes with Metallic Chirality. *Adv. Mater.* **23**, 1–5 (2011).
10. Wood, R. W. Neurobehavioral toxicity of carbon disulfide. *Neurobehav. Toxicol. Teratol.* **3**, 397–405 (1981).
11. Pean, A. R., Parsons, R. B., Waring, R. H., Williams, A. C. & Ramsden, D. B. Toxicity of sulphur-containing compounds to neuronal cell lines. *J. Neurol. Sci.* **129**, 107–108 (1995).
12. Motta, M. *et al.* The parameter space for the direct spinning of fibres and films of carbon nanotubes. *Phys. E Low-dimensional Syst. Nanostructures* **37**, 40–43 (2007).
13. Milnera, M., Kurti, J., Hulman, M. & Kuzmany, H. Periodic resonance excitation and intertube interaction from quasicontinuous distributed helicities in single-wall carbon nanotubes. *Phys. Rev. Lett.* **84**, 1324–1327 (2000).
14. Motta, M. S., Moisala, A., Kinloch, I. A. & Windle, A. H. The role of sulphur in the synthesis of carbon nanotubes by chemical vapour deposition at high temperatures. *J. Nanosci. Nanotechnol.* **8**, 2442–2449 (2008).
15. Jorio, A. *et al.* Characterizing carbon nanotube samples with resonance Raman scattering. *New J. Phys.* **5**, 139.1–139.17 (2003).
16. Fiawoo, M.-F. *et al.* Evidence of Correlation between Catalyst Particles and the Single-Wall Carbon Nanotube Diameter: A First Step towards Chirality Control. *Phys. Rev. Lett.* **108**, 1–5 (2012).
17. Schäffel, F. *et al.* Nanoengineered Catalyst Particles as a Key for Tailor-Made Carbon Nanotubes. *Chem. Mater.* 5006–5009 (2007).
18. Pang, L. S. K., Saxby, J. D. & Chatfield, S. P. Thermogravimetric analysis of carbon nanotubes and nanoparticles. *J. Phys. Chem.* **97**, 6941–6942 (1993).
19. Bom, D. *et al.* Thermogravimetric Analysis of the Oxidation of Multiwalled Carbon Nanotubes: Evidence for the Role of Defect Sites in Carbon Nanotube Chemistry. *Nano Lett.* **2**, 615–619 (2002).
20. Singh, C., Shaffer, M. S., Koziol, K. K. K., Kinloch, I. A. & Windle, A. H. Towards the production of large-scale aligned carbon nanotubes. *Chem. Phys. Lett.* **372**, 860–865 (2003).
21. Koziol, K. *et al.* High-Performance Carbon Nanotube Fiber. *Science* **318**, 1892–1895 (2007).
22. Gavillet, J. *et al.* Root-Growth Mechanism for Single-Wall Carbon Nanotubes. *Phys. Rev. Lett.* **87**, 2–5 (2001).
23. Saito, R., Hofmann, M., Dresselhaus, G., Jorio, A. & Dresselhaus, M. S. Raman spectroscopy of graphene and carbon nanotubes. *Adv. Phys.* **60**, 413–550 (2011).
24. Ferrari, A. C. Raman spectroscopy of graphene and graphite: Disorder, electron–phonon coupling, doping and nonadiabatic effects. *Solid State Commun.* **143**, 47–57 (2007).
25. Rao, A. M. & Richter, E. Shunji Bandow, Bruce Chase, P. C. Eklund, K. A. Williams, S. Fang, K. R. Subbaswamy, M. Menon, A. Thess, R. E. Smalley, G. Dresselhaus, and M. S. D. Diameter-Selective Raman Scattering from Vibrational Modes in Carbon Nanotubes. *Science* **275**, 187–191 (1997).
26. Bandow, S. *et al.* Effect of the Growth Temperature on the Diameter Distribution and Chirality of Single-Wall Carbon Nanotubes. *Phys. Rev. Lett.* **80**, 3779–3782 (1998).
27. Rao, A. M. *et al.* Effect of van der Waals Interactions on the Raman Modes in Single Walled Carbon Nanotubes. *Phys. Rev. Lett.* **86**, 3895–3898 (2001).

Acknowledgments

The authors thank the European Research Council (under the Seventh Framework Program FP7/2007-2013, ERC grant agreement no 259061) for funding this project. K.Koziol also thanks the Royal Society for further financial support. C.Paukner thanks Dr. T. Gspann for FIB analysis of samples and Nanophotonics Center, at the Cavendish Laboratory, for allowing the access to the Raman spectrometer. The authors would like to thank Dr. Francesco Bonaccorso for helpful discussion of Raman spectra.

Author contributions

C.P. wrote the main manuscript text and prepared figures 1–8. K.K.K.K. conducted HRTEM analysis. Both authors discussed results, drew conclusions and reviewed the manuscript.

Additional information

Supplementary information accompanies this paper at http://www.nature.com/scientificreports

Competing financial interests: The authors declare no competing financial interests.

How to cite this article: Paukner, C. & Koziol, K.K.K. Ultra-pure single wall carbon nanotube fibres continuously spun without promoter. *Sci. Rep.* **4**, 3903; DOI:10.1038/srep03903 (2014).